The Role of H_2S Addition on Pt/Al_2O_3 Catalyzed Propane Dehydrogenation: A Mechanistic Study

Hai-Zhi Wang [a], Wei Zhang [a], Jia-Wei Jiang [a], Zhi-Jun Sui [a,*], Yi-An Zhu [a], Guang-Hua Ye [a], De Chen [b], Xing-Gui Zhou [a], Wei-Kang Yuan [a]

[a] State Key Laboratory of Chemical Engineering, East China University of Science and Technology, Shanghai 200237, China

[b] Department of Chemical Engineering, Norwegian University of Science and Technology, N-7491 Trondheim, Norway

[*]Corresponding author. Email: zhjsui@ecust.edu.cn

Abstract

Introducing sulfur species into Pt catalysts has been proven to be an effective method to improve their performance in various reactions. However, the role of sulfur addition on Pt catalysts catalyzing propane dehydrogenation (PDH) is still not clear. This work combines catalyst characterizations, catalytic kinetics studies and DFT calculations to understand the influence of H_2S addition in the feed on Pt/θ-Al_2O_3 catalyzed PDH from a mechanistic perspective. With the addition of a trace amount of H_2S in the feed (3 ppm), the propylene selectivity increases from 79% to 96% and the deactivation factor decreases from 33% to 18%, at the expense of a slight activity loss. The improved catalytic performance can be partially attributed to the electron transfer from sulfur species to Pt atoms as indicated by CO-DRIFTS results. DFT calculations show that H_2S could be the dominating sulfur species on Pt particles and donate electrons to Pt atoms, which further proves that sulfur species improve the catalytic performance by donating electrons. In addition, the repulsion between sulfur species and C3 hydrocarbons also explains the improved catalytic performance.

keywords: H_2S addition, Pt/Al_2O_3, propane dehydrogenation, electronic structure, DFT, mechanistic study

1. Introduction

Propane dehydrogenation (PDH) is one of the most important techniques for the purposeful production of propylene, a key feedstock in the petrochemical industry.[1,2] In recent years, PDH technique receives more and more attention from both industry and academia, due to the ever-increasing demand for propylene and the abundant, cheap supply of propane from shale gas. Pt based catalysts are very efficient in catalyzing PDH reaction, and several PDH processes (e.g., UOP Oleflex and Uhde STAR) based on Pt catalysts have been commercialized.[3] PDH reaction is normally performed at the high temperature of 525-705 °C to achieve a high yield of propylene, because this reaction is highly endothermic and equilibrium limited.[4] Under this high temperature, the propylene selectivity and stability of Pt catalysts are significantly decreased, as such temperature is also favorable for various side reactions, like hydrogenolysis, deep dehydrogenation, and cracking.[5] Thus, proper approaches are required to improve the selectivity and stability of Pt catalysts for PDH.

There are several approaches available to enhance the catalytic performance of supported Pt catalysts for PDH.[6] Choosing a proper support, e.g., mesoporous alumina and TS-1, can significantly improve the catalytic performance of Pt based catalysts.[7–9] The addition of metal promoters, like Sn, Zn, Ge, Pd, In and Re, can effectively improve the propylene selectivity and stability of Pt catalysts, by modulating geometrical and electronic structures of Pt particles.[8,10–13] Besides, introducing steam, hydrogen, and sulfur species into the reaction feed is also effective in enhancing the performance of Pt catalysts for PDH.[14–17]

Among the aforementioned approaches, introducing sulfur into Pt catalysts is simple and efficient, but not yet extensively explored in the literature. Normally, sulfur is added to catalysts, through introducing sulfur species, like H_2S, thiophene, and DMDS, into the reaction feed.[15,18] Sulfur addition has been used to effectively prevent the coke formation over metal surface of dehydrogenation reactors,[19] while the knowledge of sulfur addition in Pt catalysts is still limited. Some experimental and computational works have reported the effect of sulfur addition on Pt catalysts for various reactions, such as catalytic reforming and hydrogen oxidation.[20–22] The experiments show that a high concentration of sulfur significantly deteriorates the performance of Pt catalysts by poisoning the Pt sites, while a trace amount of sulfur improves the performance of Pt catalysts through suppressing side reactions over Pt sites.[22–25] The DFT calculations display that it is very easy to dissociate H_2S to form other sulfur species over Pt surfaces and sulfur atoms strongly occupy Pt sites by chemical bonds between S and Pt.[20,26] Moreover, the chemisorbed sulfur species can lead to dramatic changes in electronic structure of Pt particles.[27]

With regards to PDH reaction, only a few experimental works have reported the effect of sulfur addition on the performance of Pt catalysts. Rennard et al.[15] added a trace amount of H_2S continuously in the feed (25-500 ppm) when using $Pt/MgAl_2O_4$ and $Pt/\eta\text{-}Al_2O_3$. They found that a sulfur addition of 425 ppm in the feed could remarkably increase the propylene selectivity of $Pt/MgAl_2O_4$ from 47% to 95% without changing its activity, and the sulfur addition could also increase the propylene selectivity of $Pt/\eta\text{-}Al_2O_3$. Jackson et al.[23] explored three ways of sulfur addition in

Pt/Al_2O_3 (5.6×10^{17} - 6.696×10^{20} S atoms/g_{cat}), namely, adding sulfuric acid in the catalyst preparation stage, predosing the catalyst with H_2S, and co-feeding of H_2S and propane during reaction. They concluded that all the three ways of sulfur addition could improve the propylene selectivity of Pt/Al_2O_3 and this selectivity was not directly related to the amount of sulfur on the catalyst surface. Up to now, the interaction between sulfur species and Pt catalysts for PDH and its influence on catalyst performance have not yet been revealed.

In this work, combining experiments and DFT calculations, the role of sulfur addition on $Pt/\theta\text{-}Al_2O_3$ catalyzed PDH was investigated from a mechanistic perspective. The sulfur is added into the catalyst through co-feeding H_2S with reactants, which is commonly used in the industry. With different concentrations of H_2S in the feed (0-9 ppm), the as-synthesized $Pt/\theta\text{-}Al_2O_3$ catalyst was tested for PDH reaction. The geometrical and electronical structures of the fresh and spent $Pt/\theta\text{-}Al_2O_3$ catalysts were characterized by HAADF-STEM, CO-Chemisorption, and CO-DRIFTS. Besides, DFT calculations were performed to analyze the adsorption of sulfur species on Pt surfaces, the electronic structure of Pt surfaces with sulfur species adsorbed, the adsorption of propylene, and the activation energies of PDH.

2. Experimental Section

2.1 Catalyst preparation

A $Pt/\theta\text{-}Al_2O_3$ catalyst was prepared by using the incipient wetness impregnation

method. θ-Al_2O_3 is usually used as the support of Pt catalysts for commercial PDH processes, due to its high thermal stability and mechanical strength, as well as its ability to highly disperse Pt particles.[4,28] θ-Al_2O_3 was obtained by calcinating pseudo-boehmite (Aldrich) at 1000 °C for 6 h in static air with a heating rate of 3 °C/min.[29] Then, θ-Al_2O_3 was loaded with 0.5 wt% Pt using a solution of H_2PtCl_6 (Sinopharm). After the impregnation, the sample was aged at room temperature for 12 h, dried at 120 °C for 8 h, and calcined at 500 °C for 4 h with a heating rate of 2 °C/min. The properties of the as-synthesized Pt/θ-Al_2O_3 were summarized in Table 1.

Table 1. Properties of the as-synthesized Pt/θ-Al_2O_3 catalyst

S_{BET} [a] (m^2/g)	d_{pore} [a] (nm)	Pt loading [b] (wt%)	Pt dispersion [c] (%)	D_{Chem} [c] (nm)	D_{TEM} [d] (nm)
103	14.0	0.5	78.2	1.2	0.9

[a] Determined from the nitrogen adsorption-desorption isotherm.
[b] Determined by ICP-AES.
[c] Determined by CO-Chemisorption.
[d] Determined from HAADF-STEM.

2.2 Catalytic tests

With different concentrations of H_2S in the reaction feed (i.e., 0, 3, and 9 ppm), the PDH reaction was carried out in a μ-BenchCAT reactor (Altamira Instrument, USA) equipped with a quartz tube with an inner diameter of 6 mm. For each catalytic test, 0.1 g of the catalyst was loaded in the quartz tube. All the catalytic tests were conducted at the temperature of 575 °C, propane partial pressure of 12 kPa, C_3H_8:H_2 molar ratio of 1:2, total pressure of 1 atm with Ar as the balance gas, and total flow rate of 90 ml/min. A mixture of H_2S and Ar (30 ppm) was continuously introduced

into the reaction feed to achieve a specific concentration of H_2S. The effluent gas was analyzed online with a 4-channel microgas chromatograph (INFICON 3000, USA).[30]

To determine the activation energies of different catalysts, the PDH reaction was performed under different temperatures (i.e., 535, 555, 575, and 595 °C), and the other reaction conditions were the same as the above catalytic tests. Besides, 0.02 g of Pt/θ-Al_2O_3 catalyst was loaded in the reactor to achieve a conversion of propane well below the equilibrium one.

The propane conversion (C), propylene selectivity (S), and deactivation parameter (D)[31] were calculated by:

$$C = \frac{F_{C_3H_8,f} - F_{C_3H_8,o}}{F_{C_3H_8,f}} \times 100\% \quad (1)$$

$$S = \frac{F_{C_3H_6,o}}{\sum_i \frac{n_i}{3} F_{i,o}} \times 100\% \quad (2)$$

$$D = \frac{C_{init} - C_{end}}{C_{init}} \times 100\% \quad (3)$$

Here, $F_{C3H8,f}$ is the flow rate of propane in the feed; $F_{C3H8,o}$, $F_{C3H6,o}$, and $F_{i,o}$ are the flow rates of propane, propylene, and component i in the outlet; n_i is the carbon number of component i; C_{init} and C_{end} are the initial and final conversions of propane. The deactivation parameter (D) was used to quantify the stability of a catalyst.

2.3 Catalyst characterization

Nitrogen adsorption-desorption isotherm measurements were performed at -196 °C, using an ASAP 2020 HD apparatus (Micromeritics, USA). Prior to the

measurements, the samples were degassed at 350 °C and 1.33×10^{-3} Pa for 6 h. CO chemisorption was carried out on an Autochem 2920 instrument (Micrometrics, USA), equipped with a thermal conductivity detector. High-angle annular dark-field scanning transmission electron microscopy (HAADF-STEM) images were taken using a Tecnai G2 F20 S-Twin instrument (FEI, USA) operated at 200 kV. The thermogravimetric analysis (TG) was conducted on a Pyris 1 instrument (Perkin-Elmer, USA), with temperature increasing from room temperature to 800 °C at a heating rate of 10 °C/min. The elemental analysis was performed on a Vario EL III elemental analyzer (Elementar, Germany).

The diffuse reflectance infrared Fourier transform spectroscopy (DRIFTS) study was carried out on a PerkinElmer Spectrum 100 FT-IR spectrometer (Perkin Elmer, USA), which was equipped with a liquid nitrogen cooled mercury-cadmium-telluride (MCT) detector and an in situ Harrick Praying Mantis diffuse reflectance cell. The DRIFT spectra were recorded with an accumulation of 32 scans and a spectral resolution of 4 cm^{-1}.[32] The catalyst powder (~50 mg) was firstly reduced in flowing hydrogen (20 ml/min) at 550 °C for 1.5 h, and then treated with H_2S (3 ppm and 9 ppm, respectively) under the same H_2 flow rate, total flow rate and temperature with the catalytic tests, followed by being cooled down to 30 °C in flowing Ar (20 ml/min) for 0.5 h. After that, a background spectrum was recorded. Then, the catalyst was exposed to pure CO (20 ml/min) at 30 °C for 0.5 h and purged with Ar (20 ml/min) until no gas-phase CO was detected in the FT-IR spectrum, and this FT-IR spectrum of the catalyst treated with H_2S was collected for analysis. Without the treatment with

H_2S, the above steps were repeated to obtain the FT-IR spectrum for comparison.

2.4 Computational method

All the density functional theory (DFT) calculations were carried out using the VASP package with the general gradient approximation (GGA) BEEF-vdW functional.[33–35] The interactions between valence electrons and ion cores were determined by Blöchl's all-electron-like projector augmented wave (PAW) method.[36] A plane wave energy cut-off of 400 eV was employed to ensure a tight convergence. Brillouin zone sampling was conducted using a Monkhorst-Pack grid with respect to the symmetry of the system, and the electronic occupancies were calculated according to the Methfessel-Paxton scheme[34] with an energy smearing of 0.2 eV.

The Pt(111) surface was represented by a five-layer slab with a p(3 × 3) supercell and the Pt(211) surface was represented by a (1 × 3) unit cell with five layers, in which the equilibrium Pt-Pt interatomic distance was 2.82 Å.[36] The successive slabs were separated by a vacuum region of 12 Å to avoid periodic interactions. Monkhorst Pack mesh of 5 × 5 × 1 and 5 × 3 × 1 *k*-points sampling in the surface Brillouin zone were used on the Pt(111) and Pt(211) surfaces, respectively. For both Pt(111) and Pt(211) surfaces, the bottom two layers were fixed. The ground-state atomic geometries of bulk and surfaces were determined by minimizing the Hellman-Feynman forces with the conjugate-gradient algorithm until the force on each ion was below 0.03 eV/Å.

The adsorption energy (E_{ads}) of an adsorbate was calculated by the following equation:

$$E_{ads} = E_{adsorbate/substrate} - E_{adsorbate} - E_{substrate} \quad (4)$$

where E_x is the DFT total energy of a X system. A negative E_{ads} reflects an energy gain when X adsorbs on the substrate. Bader charge analysis was conducted to evaluate electron transfer between sulfur species and Pt atoms. Transition states were found by using the dimer method, in which the most stable configurations of reactants on Pt surfaces obtained from the standard DFT minimization were used as the initial states. The convergence was regarded to be achieved with the force on each atom less than 0.03 eV/Å.

3. Results and Discussion

3.1 Effect of H_2S addition on PDH and coke formation

The catalytic performance of Pt/θ-Al_2O_3 with different concentrations of H_2S in the reaction feed (i.e., 0, 3, and 9 ppm) is displayed in Fig. 1. The initial propane conversion decreases from 21.8% to 14.9% with the increase of H_2S concentration from 0 to 9 ppm, indicating the addition of H_2S can poison the catalyst. Besides, the propane conversions decay with reaction time, which is commonly believed to be caused by deactivation by coking. Without H_2S addition in the feed, the catalyst deactivates more quickly, with a deactivation parameter (see Eq. (3)) of 33%; when 3 and 9 ppm H_2S are added into the feed, the deactivation parameter for the catalyst is 18% and 25%, respectively. This result implies that H_2S may modify the catalyst and

subsequently suppress the catalyst deactivation by coking, and an excessive addition of H_2S (> 9 ppm) may reduce the stability of the Pt catalyst. Fig. 1b displays a remarkable increase of the initial propylene selectivity from 58.4% to 83.8% when changing H_2S concentration from 0 to 3 ppm, and the propylene selectivity reaches 96% after 4 h of reaction. Besides, the propylene selectivity is not sensitive to the concentration of H_2S within the range of 3-9 ppm. Apparently, the addition of H_2S can significantly increase the propylene selectivity and stability of Pt/θ-Al_2O_3, although a slight activity loss is also observed.

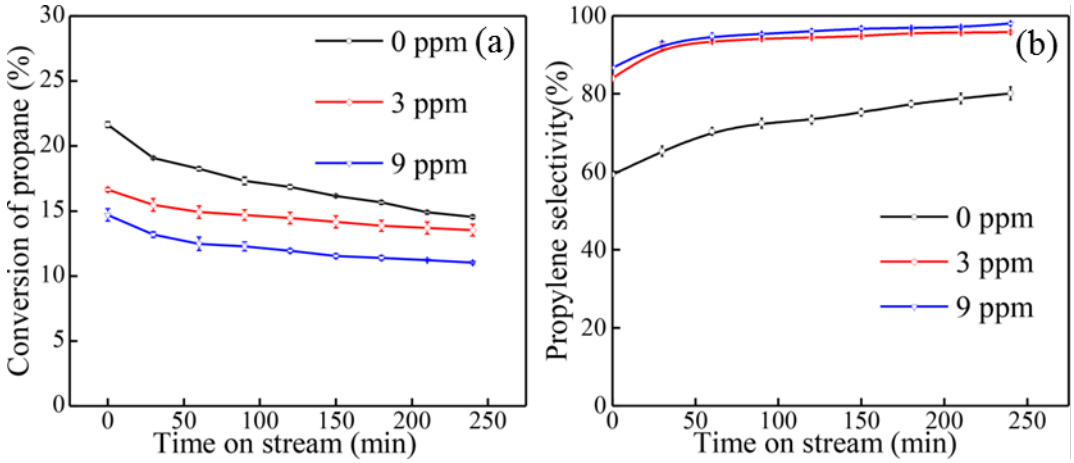

Figure 1. (a) Propane conversion and (b) propylene selectivity of Pt/θ-Al_2O_3 with different concentrations of H_2S in the reaction feed (i.e., 0, 3, and 9 ppm). Reaction conditions: 0.1 g catalyst, P_t = 1 atm, T = 575 ºC, and H_2/C_3H_8 = 2.

The coke on the spent Pt/θ-Al_2O_3 catalysts was characterized by TG and elemental analysis, and the results are displayed in Table 2. The coke amount decreases from 3.3 to 2.1 wt% with the increase of H_2S concentration from 0 to 9 ppm, indicating the addition of H_2S can suppress coke formation reactions. Besides, the

coke index (Ψ = coke content/yield of propene) is introduced to rule out the effect of different propane conversions, and the same result is observed, which further proves that the presence of H_2S can make the catalyst more resistant to coking. The elemental analysis shows that the H/C ratio of coke increases from 0.62 to 1.25 with the increase of H_2S concentration from 0 to 9 ppm.[37,38] This result indicates that the deep dehydrogenation reactions are inhibited when introducing H_2S in the reaction feed, which would lead to the formation of less deeply dehydrogenated coke precursors and suppress the coking reaction associated with these coke precursors.[39]

Table 2. Properties of the spent Pt/θ-Al_2O_3 catalysts collected after 4 h of reaction

Samples	Coke content (wt %)	Ψ [a] ($mg/(g_{cat} \times g_{C3H6})$)	H/C ratio	Accessible Pt atoms/Total Pt atoms[b] (%)	TOF (s^{-1})
0 ppm H_2S	3.3	0.30	0.62	10	1.51
3 ppm H_2S	2.8	0.21	0.85	13	1.18
9 ppm H_2S	2.1	0.18	1.25	12	1.06

[a] Ψ represents the coke index (coke content/yield of propylene).

[b] The ratio of accessible Pt atoms to total Pt atoms is determined by CO-Chemisorption.

3.2. Effect of H_2S addition on catalyst structures

3.2.1 HAADF-STEM

Fig. 2 shows the representative HAADF-STEM images of the fresh catalyst sample and the spent catalyst samples collected after 4 h of PDH reaction. The Pt particles in the fresh sample are highly dispersed with an average diameter of 0.9 nm. After 4 h of reaction with 0, 3, and 9 ppm of H_2S in the feed, the average particle diameters all grow to 1.2 nm. Apparently, the H_2S addition has a negligible effect on Pt particle size, indicating the distinct catalyst performance (see Fig. 1) is not caused

by different Pt particle sizes.

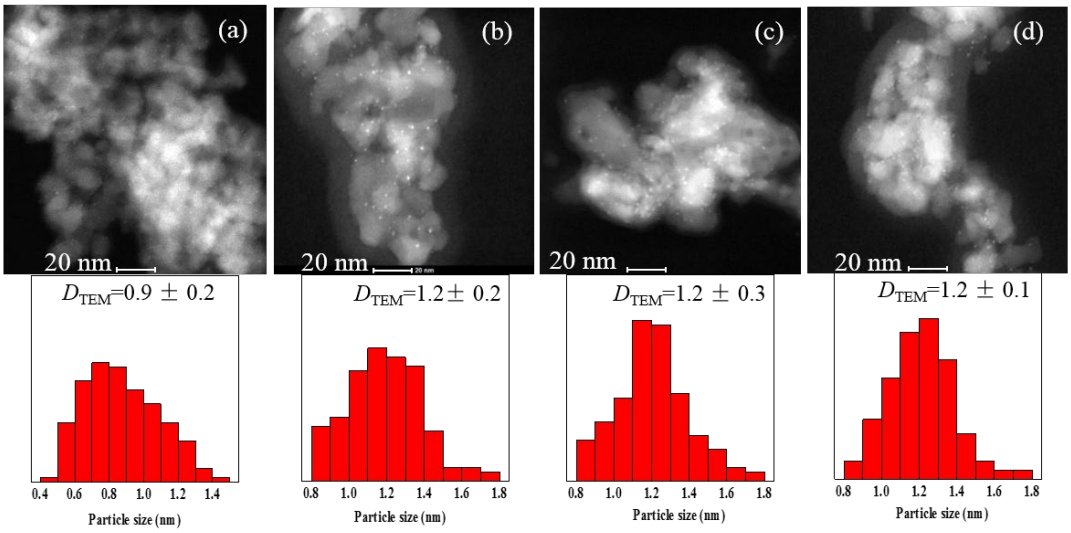

Figure 2. HAADF-STEM images and particle size distributions of (a) the fresh catalyst and the spent catalysts collected after 4 h of PDH reaction with (b) 0 ppm H_2S, (c) 3 ppm H_2S, and (d) 9 ppm H_2S in the reaction feed.

3.2.2 CO chemisorption

Table 2 gives the ratio of accessible Pt atoms to total Pt atoms of the spent catalyst samples collected after 4 h of reaction. Compared to the fresh sample (see Table 1), the number of accessible Pt sites of all spent samples decreases largely, due to the accumulation of coke and sulfur species on Pt particles. The ratio of accessible Pt atoms to total Pt atoms of the spent catalyst with H_2S addition is 20%-30% higher than of the spent catalyst without H_2S addition, which could be ascribed to the less coke amount on the samples (see Table 2). Besides, Table 2 shows that the TOF decreases with the addition of H_2S in the reaction feed. According to the literature,[27] the chemisorbed sulfur species affect the electronic structure of Pt particles, which

could be one reason for the decreased TOF. To acquire the effect of H_2S on the electronic structure of Pt particles, CO-DRIFTS measurements were performed.

3.2.3 CO-DRIFTS

Fig. 3 shows the CO-DRIFTS spectra of the Pt/θ-Al_2O_3 catalysts treated and untreated with H_2S. For the spectrum of the catalyst untreated with H_2S, three adsorption peaks in the range of 2040-2090 cm^{-1} are observed, and they can be ascribed to the linear-bonded CO on Pt atoms. Specifically, the highest energy band at 2084 cm^{-1} represents the CO linearly bound to highly coordinated Pt sites, the band at 2065 cm^{-1} represents the CO linearly adsorbed on the terraces of Pt particles, and the lowest one at 2045 cm^{-1} represents the CO linearly adsorbed at the corners.[40–42] After the catalyst is treated with 3 ppm H_2S, the three bands show a downward shift, changing from 2084 to 2077 cm^{-1}, 2065 to 2059 cm^{-1}, and 2045 to 2040 cm^{-1}, respectively. When the catalyst is treated with 9 ppm H_2S, the three bands also show a downward shift, changing from 2084 to 2082 cm^{-1}, 2065 to 2064 cm^{-1}, and 2045 to 2042 cm^{-1}, respectively. The downward shift indicates Pt-CO bond is strengthened while C-O bond is weakened, which is because the electron density over Pt atoms increases and thus more Pt electrons back-donate into the $2\pi^*$ anti-bonding orbital of CO molecules.[31,43] The adsorbed sulfur species on Pt surfaces can transfer electrons to Pt atoms and make their electron density enhanced, which would be validated by DFT calculations in the section 3.4.2. These electron-rich Pt particles are favorable for desorption of propylene, and thus inhibit side reactions, including coke formation. Compared to the catalyst treated with 3 ppm H_2S, the catalyst treated with 9 ppm H_2S

displays an upward shift of the CO bands. Since H_2S can be easily dissociated to form S atoms on Pt particles,[44] the number of S deposited on Pt particles and the poisoning rate increase with the elevated concentration of H_2S in the feed.[45] The adsorbed S can act as an electron acceptor molecule on the Pt surfaces and decrease the Pt-CO interaction, which was confirmed in the literature.[46]

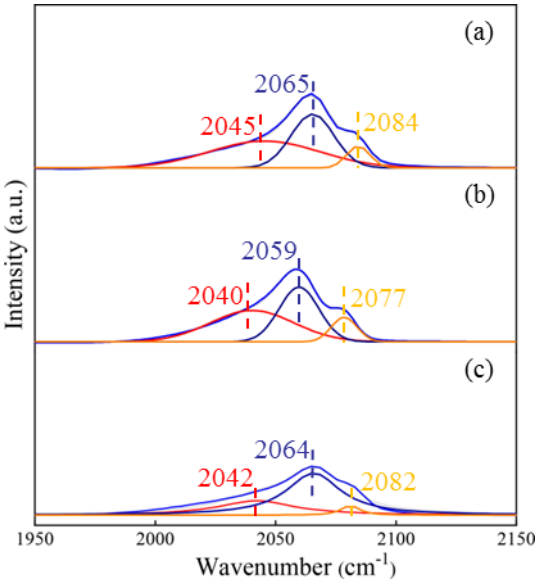

Figure. 3. DRIFTS of CO adsorption on (a) the Pt/θ-Al_2O_3 catalyst untreated with H_2S, (b) the Pt/θ-Al_2O_3 catalyst treated with 3 ppm H_2S, and (c) the Pt/θ-Al_2O_3 catalyst treated with 9 ppm H_2S.

3.3 Effect of H_2S addition on activation energy

To further explore the effect of H_2S addition in the feed on the Pt/θ-Al_2O_3 catalyzed PDH, the activation energies are determined in the Arrhenius plots (see Fig. 4). The activation energy of the catalysts in this work is in the range of 60-120 kJ/mol, which is reasonable compared to the results reported in the literature.[2,47,48] The activation energy for the catalyst without H_2S addition is 62 kJ/mol, while the ones

for the catalysts with 3 and 9 ppm of H_2S addition increase to 71 kJ/mol and 78 kJ/mol, respectively. Since the activation energy would decrease with less coke deposited on Pt surfaces during PDH based on the literatures,[14,49,50] the increase of activation energy in this work could be ascribed to the presence of H_2S, and this effect was investigated by DFT calculations in section 3.4.4.

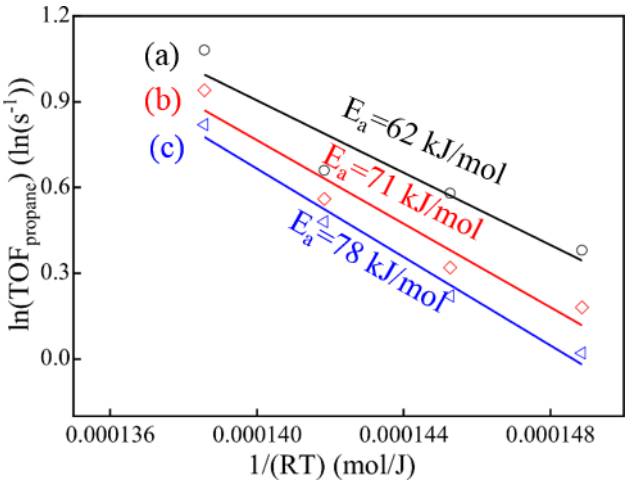

Figure 4. Arrhenius plots of TOFs. (a) The Pt/θ-Al_2O_3 catalyst without H_2S addition in the feed, (b) the Pt/θ-Al_2O_3 catalyst with 3 ppm of H_2S in the feed, and (c) the Pt/θ-Al_2O_3 catalyst with 9 ppm of H_2S in the feed.

3.4. DFT results

From the above experimental results, the addition of H_2S in the feed can significantly improve the performance of Pt/θ-Al_2O_3 and changes the electronic structure of Pt particles. However, the mechanistic insights into the effect of sulfur addition on Pt/θ-Al_2O_3 catalyzed PDH are still lacking. In this section, with the aid of DFT calculations, how sulfur species are adsorbed on Pt surfaces is analyzed, the effects of sulfur species on the electronic structure of Pt surfaces and the adsorption of

propylene on Pt surfaces are determined, and the effect of sulfur species on the activation energies of PDH elementary steps is obtained.

3.4.1 Adsorption of sulfur species

Possible sulfur species on Pt surfaces are S, SH, and H_2S,[20] and their favorable adsorption sites and corresponding adsorption energies are displayed in Table 3. The most favorable adsorption sites for S, SH, and H_2S are fcc, bridge, and atop sites on Pt(111), and hcp, bridge, and atop sites on Pt(211); their corresponding adsorption configurations are displayed in Fig. S1 in the Supporting Information. The adsorption strength of sulfur species on Pt(111) and Pt(211) shows a decreasing trend in S > SH > H_2S, which coincides with the results reported in the literature.[20,51] The adsorption energies of S on Pt(111) and Pt(211) are -4.98 eV. The adsorption energies of SH (-2.9 eV) and H_2S (-0.83 eV) on Pt(111) are lower than the ones of SH (-3.43 eV) and H_2S (-0.97 eV) on Pt(211), indicating SH and H_2S are more easily adsorbed on Pt(211). Compared to Pt(111), Pt(211) tends to catalyze side reactions in PDH, e.g., deep dehydrogenation and cracking of C3 derivatives.[50] Thus, the adsorption of sulfur species on Pt(211) can significantly suppress side reactions and subsequently improve propylene selectivity.

Table 3. Adsorption energies and favorable sites of sulfur species on Pt(111) and Pt(211) surfaces

Species	Pt (111)		Pt (211)	
	Favorable site	ΔE (eV)	Favorable site	ΔE (eV)
S	fcc	-4.98	hcp	-4.98
SH	bridge	-2.90	bridge	-3.43
H_2S	atop	-0.83	atop	-0.97

3.4.2 Electron structure analysis

Bader charge analysis results are displayed in Fig. 5 and the amount of transferred electrons from sulfur species is summarized in Table 4. In Fig. 5, the blue regions represent electron depletion, while the yellow regions represent electron accumulation. For the configuration of S adsorption on Pt(111) and Pt(211), the electron depletion region is primarily located on the three sides below the S atom and the electron accumulation region is above the S atom, which means S gains electron from Pt(111) and Pt(211) (see Table 4). However, H_2S donates 0.27 electrons to Pt(111) and 0.24 electrons to Pt(211), with its electron depletion region upright above the S atom and its electron accumulation region on Pt atoms.[52] Compared to H_2S, negligible electrons are transferred from SH to Pt surfaces. The number of charge transferred from SH to Pt atoms is between the ones of H_2S and S, and the similar result is found for the adsorption energies (see Table 3). Normally, the strength of the interaction between adsorbate and substrate is related to charge transfer. In this work, the adsorption strength of sulfur species on Pt(111) and Pt(211) shows a decreasing trend in S > SH > H_2S, while the number of charge transferred from sulfur species to Pt atoms exhibits an increasing order in S < SH < H_2S. It should be noted that the adsorption strength is not solely related to charge transfer and it can also be affected by adsorption sites, adsorbate, and direction of charge transfer. For example, Li reported that the adsorption energy of NH_3 is lower than the adsorption energy of H_2O on the Ts site even if the number of charge transfer from NH_3 to metal surface is more

than the one from H_2O to metal surface.[53,54]

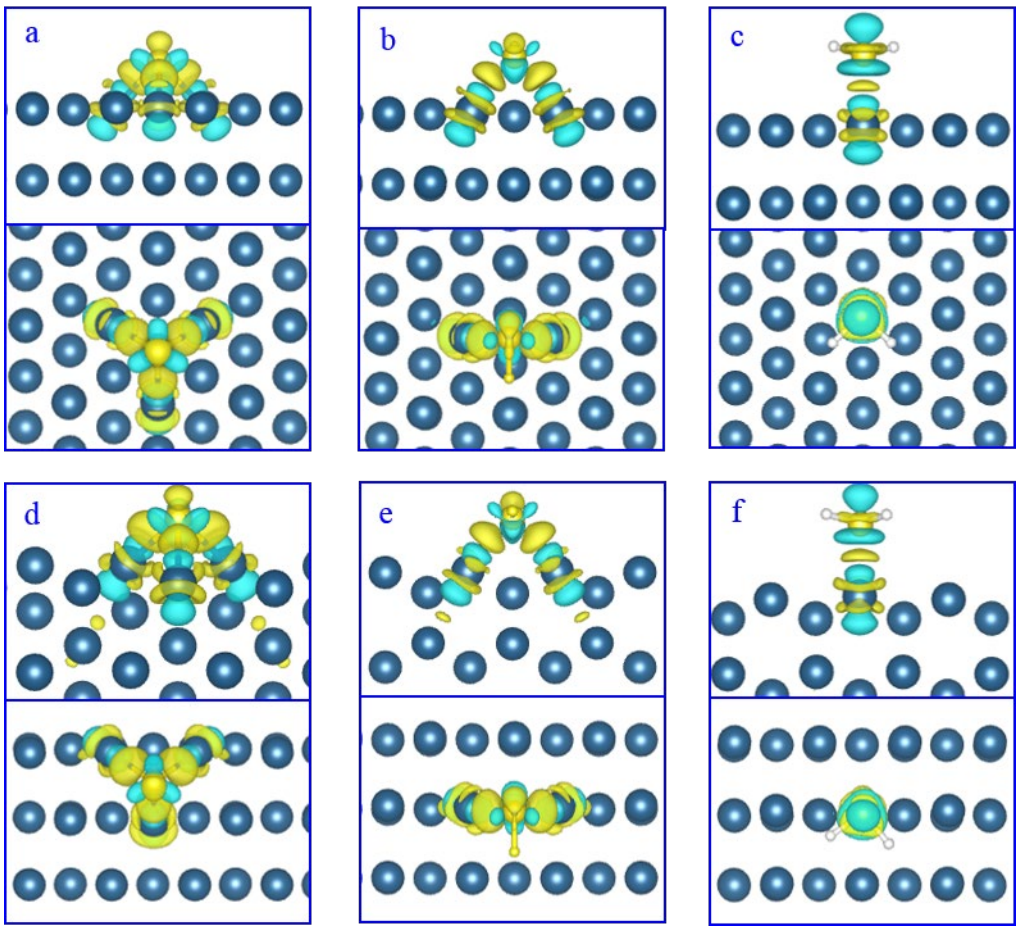

Figure 5. Bader charge analysis of the Pt(111) surface adsorbed with (a) S, (b) SH, and (c) H_2S, as well as the Pt(211) surface adsorbed with (d) S, (e) SH, and (f) H_2S. Side and top views are given, Pt atoms are in blue, S atoms are in yellow, and H atoms are in gray.

Table 4. The amount of electrons transferred from Pt surface to S, SH, and H_2S

Species	Pt (111)		Pt (211)	
	Favorable site	Δq	Favorable site	Δq
S	fcc	+0.09	hcp	+0.13
SH	bridge	-0.02	bridge	0
H_2S	atop	-0.27	atop	-0.24

For Δq, the "+" and "-" denote sulfur species gain and lose electrons, respectively.

The CO-DRIFTS study in our work indicates that the electron density over Pt atoms increases in the presence of 3 ppm H_2S and extensive H_2. Under this condition, S could be converted into SH and H_2S on Pt particles even though H_2S can easily dissociate on the Pt(111) surface, and the same phenomenon was also observed on other metals, such as Co.[27,55,56] Based on this knowledge and results from Bader charge analysis, H_2S can be tentatively regarded as dominating sulfur species on Pt particles in the CO-DRIFTS study as well as the catalytic tests, since the two experiments were performed at the similar conditions. To consolidate that H_2S is the dominating sulfur species on Pt particles, the CO adsorption energies on the clean Pt(111), the Pt(111) with co-adsorbed sulfur species, the clean Pt(211), and the Pt(211) with co-adsorbed sulfur species are calculated, as shown in Table 5. The most favorable adsorption site of CO on Pt(111) is fcc site and the one on Pt(211) is bridge site, which is consistent with the results reported in the literature.[57,58] The adsorption energy of CO on Pt (111) (-1.62 eV) is higher than that on Pt(111)&S (-1.52 eV) and that on Pt(111)&SH (-1.59 eV), but lower than that on Pt(111)&H_2S (-1.67 eV). Similarly, the adsorption energy of CO on Pt (211) (-1.90 eV) is higher than that on Pt(211)&S (-1.70 eV) and that on Pt(211)&SH (-1.71 eV), but lower than that on Pt(211)&H_2S (-2.04 eV). These results indicate Pt-CO bond is only strengthened when H_2S is adsorbed on Pt surfaces, which consolidates that H_2S is the dominating sulfur species on Pt particles.

When H_2S is the dominating sulfur species on Pt particles, the Pt catalyst benefits most. The adsorption energy of H_2S is the lowest (see Table 3), which could reduce

the deactivation by sulfur deposition; H_2S transfers most electrons to Pt atoms (see Table 4), which could promote desorption of propylene and subsequently suppress side reactions, including coke formation.

Table 5. CO adsorption energies on the clean Pt(111), the Pt(111) with co-adsorbed sulfur species, the clean Pt(211), and the Pt(211) with co-adsorbed sulfur species

Surface	Site	ΔE_{ads} (eV)
Pt(111)	fcc	-1.62
Pt(111)&S	bridge	-1.52
Pt(111)&SH	hcp	-1.59
Pt(111)&H_2S	fcc	-1.67
Pt(211)	bridge	-1.90
Pt(211)&S	atop	-1.70
Pt(211)&SH	atop	-1.71
Pt(211)&H_2S	bridge	-2.04

3.4.3 Adsorption energy of propylene

The adsorption energies of propylene on the clean Pt(111) and the Pt(111) with co-adsorbed sulfur species are compared in Fig. 6. Our previous work has proven that the adsorption of propylene on Pt(111) and Pt(211) is more favorable in the di-σ mode than in the π mode.[59] Fig. 6 shows that the adsorption of propylene on Pt(111) and Pt(211) is also in the di-σ mode and the adsorption energy is -1.12 eV and -1.37 eV. With the co-adsorption of S, SH, and H_2S on Pt(111) surface, the favorable adsorption mode of propylene does not change, but the adsorption energy decreases to -0.99 eV, -0.8 eV, and -0.72 eV, respectively. On Pt(211)&H_2S, the favorable adsorption of propylene is in the di-σ mode; on Pt(211)&SH and Pt(211)&S, the favorable adsorption configuration changes to the π mode. This change of adsorption

configuration is induced by the space limitation on Pt(211). Meanwhile, the adsorption energy of propylene decreases to -1.16, -1.19, and -1.22 eV on Pt(211)&H_2S, Pt(211)&SH, and Pt(211)&S. With H_2S adsorbed on Pt(111) and Pt(211), the Pt atoms are electron-rich and thus tend to repulse the electron-rich propylene, yielding significantly decreased adsorption energy of propylene.[60,61] With SH and S adsorbed on Pt(111) and Pt(211), these sulfur species do not donate electrons to Pt atoms, but the adsorption energy of propylene is also decreased. This can be ascribed to the repulsion between sulfur species and propylene. Thus, apart from the repulsion between electron-rich Pt atoms and propylene, the repulsion between sulfur species and propylene can also improve the performance of Pt catalysts.

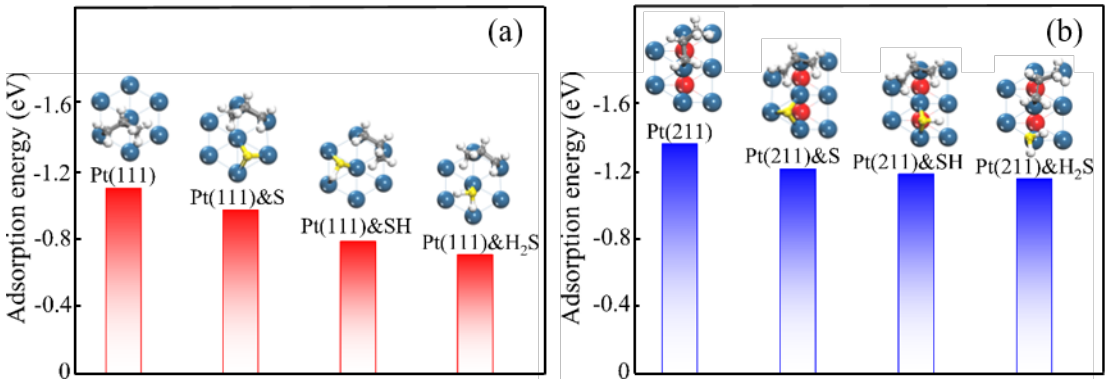

Figure 6. Adsorption energies of propylene (a) on the clean Pt(111) and the Pt(111) co-adsorbed with sulfur species, and (b) the clean Pt(211) and the Pt(211) co-adsorbed with sulfur species.

3.4.4 Activation energies of elementary reaction steps

PDH reaction contains two dehydrogenation steps: (1) C-H cleavage from methyl

or methylene groups, yielding 1-propyl or 2-propyl; (2) dehydrogenation of 1-propyl or 2-propyl to propylene. Our previous work has proven that the activation energy barrier for C-H cleavage from methyl group resembles that for C-H cleavage from methylene group.[62] Thus, the activation of C-H bond in the methylene group is investigated. Fig. 7 presents the transition state structures for PDH reaction on the clean Pt(111) and the Pt(111) with co-adsorbed sulfur species. In step (1), propane is dehydrogenated at an atop site, the detached H atom is positioned at a bridge site, the activated C-H bond is elongated to 1.60-1.68 Å, and the 2-propyl is located at an atop site. In step (2), the configurations of the transition states resemble the adsorption configuration of propylene and the activated C-H bond is elongated to 1.53-1.56 Å. The similar results for the Pt(211) surfaces can be found in Fig. S2 in the Supporting Information.

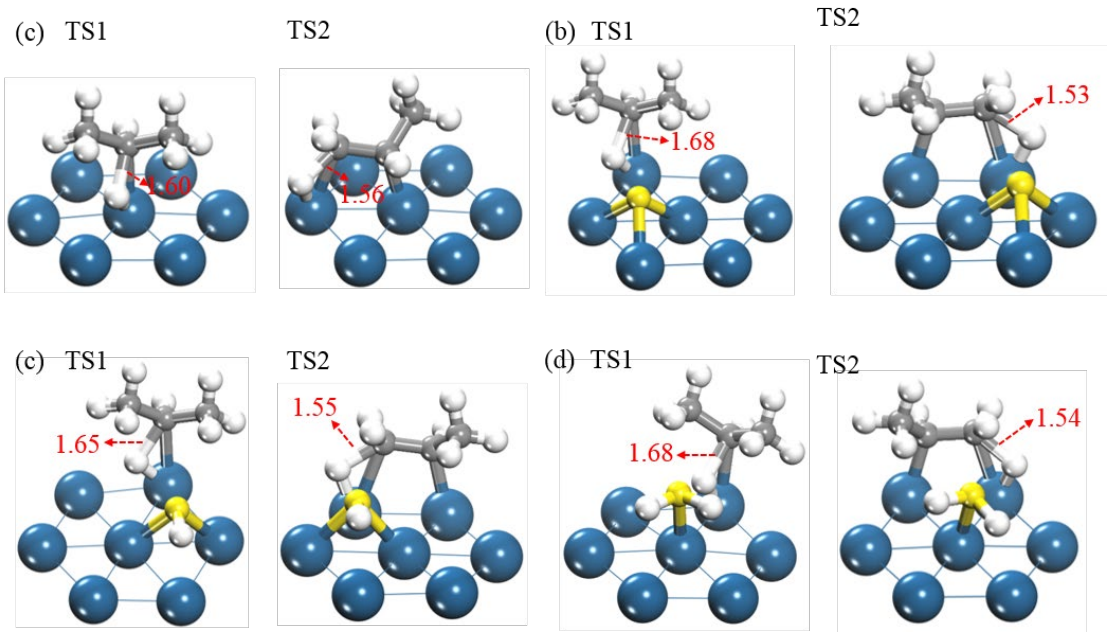

Figure 7. Transition state structures for PDH reaction over (a) Pt(111), (b) Pt(111)&S, (c) Pt(111)&SH, and (d) Pt(111)&H_2S.

The activation energies for the two dehydrogenation steps on the different Pt(111) and Pt(211) surfaces are presented in Fig. 8. With sulfur species co-adsorbed on Pt(111) and Pt(211), the activation energies for the two steps all increase significantly. Among these sulfur species, H_2S has the strongest influence on the activation energies of the two steps, with the activation energy for the first step increasing from 0.92 eV (Pt(111)) to 1.40 eV (Pt(111)&H_2S) and from 0.64 eV (Pt(211)) to 0.96 eV (Pt(211)&H_2S), and the one for the second step increasing from 0.89 eV (Pt(111)) to 1.13 eV (Pt(111)&H_2S) and from 0.64 eV (Pt(211)) to 0.79 eV (Pt(211)&H_2S). For the Pt(111) and Pt(211) co-adsorbed with H_2S, the electron-rich Pt atoms and the repulsion between sulfur species and C3 hydrocarbons weaken the binding strength of C3 hydrocarbons and simultaneously suppress the bond breaking reactions on Pt surfaces, which explains the increased activation energies required to break the C-H bonds in the two dehydrogenation steps. For the Pt(111) and Pt(211) with S and SH, the strong repulsion between sulfur species and C3 hydrocarbons could explain the increased activation energies. The elevated activation energies for Pt(111) and Pt(211) with co-adsorbed sulfur species may lead to the decreased activity. In our previous work, with oxygenated species co-adsorbed on Pt(111), the similar result in activation energies was found and the catalyst activity also decreased.[63]

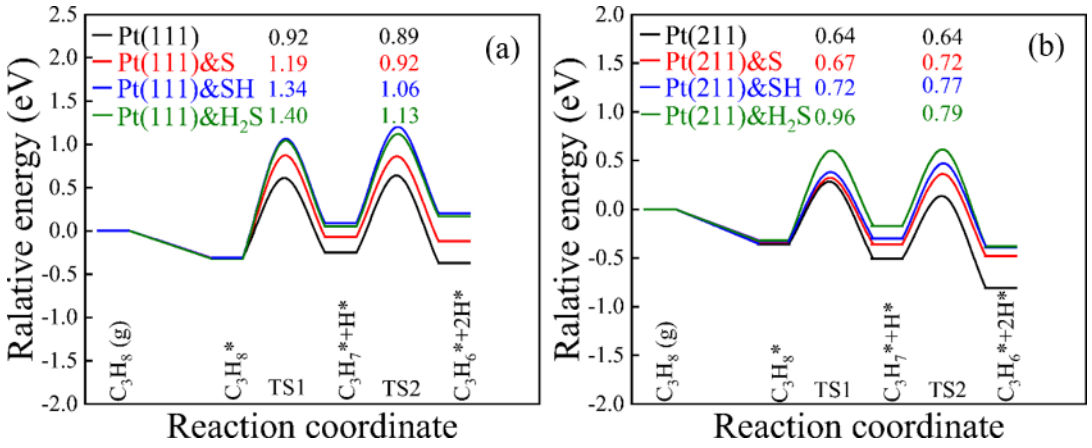

Figure 8. Reaction pathways and activation energies of PDH reaction over the clean Pt(111), Pt(111)&S, Pt(111)&SH, and Pt(111)&H_2S.

4. Conclusions

In this work, integrating experiments and DFT calculations, we provided the mechanistic insights into the effect of H_2S addition in the feed on the Pt/θ-Al_2O_3 catalyzed propane dehydrogenation (PDH). With the addition of 3 ppm H_2S in the feed, the propylene selectivity of the catalyst increases from 79% to 96%, the deactivation factor decreases from 33% to 18%, the coke amount deceases from 3.3 wt% to 2.8 wt%, and the activity is only slightly reduced. HAADF-STEM displays that the Pt particle size is almost unchanged with the introduction of H_2S in the feed, while CO-DRIFTS analysis indicates sulfur species can donate electrons to Pt atoms. DFT calculations reveal that sulfur species prefer to be adsorbed on Pt(211) when compared to Pt(111). Combining CO-DRIFTS and Bader charge analysis, H_2S could be the dominating sulfur species adsorbed on Pt particles and it donates electrons to Pt atoms, when compared to S and SH. Due to the repulsion between electron-rich Pt atoms and C3 hydrocarbons as well as the repulsion between sulfur species and C3

hydrocarbons, the adsorption energy of propylene decreases with sulfur species co-adsorbed on Pt particles, which suppresses side reactions and subsequently improves the selectivity and stability of the Pt catalyst. These repulsions also make the activation energies for the elementary dehydrogenation steps increase significantly, when sulfur species are co-adsorbed on Pt particles.

These results in this work provide a comprehensive and in-depth understanding of the role H_2S addition in improving Pt catalysts for PDH, which should be used to guide the development of Pt catalysts with high performance.

Acknowledgements

This work was financially supported by National Key R&D Program of China (2018YFB0604700), National Natural Science Foundation of China (91645122) and the "Chenguang Program" supported by Shanghai Education Development Foundation and Shanghai Municipal Education Commission (17CG29).

References

1 Q. Li, Z. J. Sui, X. G. Zhou, Y. A. Zhu, J. H. Zhou and D. Chen, *Top. Catal.*, 2011, **54**, 888–896.

2 J. Zhu, M. L. Yang, Y. Yu, Y. A. Zhu, Z. J. Sui, X. G. Zhou, A. Holmen and D. Chen, *ACS Catal.*, 2015, **5**, 6310–6319.

3 Z. Nawaz, *Rev. Chem. Eng.*, 2015, **31**, 413–436.

4 J. J. H. B. Sattler, J. Ruiz-Martinez, E. Santillan-Jimenez and B. M. Weckhuysen, *Chem. Rev.*, 2014, **114**, 10613–10653.

5 B. K. Vu, M. B. Song, I. Y. Ahn, Y. W. Suh, D. J. Suh, J. S. Kim and E. W. Shin, *J. Ind. Eng. Chem.*, 2011, **17**, 71–76.

6 A. Iglesias-Juez, A. M. Beale, K. Maaijen, T. C. Weng, P. Glatzel and B. M. Weckhuysen, *J. Catal.*, 2010, **276**, 268–279.

7 J. Li, J. Li, Z. Zhao, X. Fan, J. Liu, Y. Wei, A. Duan, Z. Xie and Q. Liu, *J. Catal.*, 2017, **352**, 361–370.

8 G. Siddiqi, P. P. Sun, V. Galvita and A. T. Bell, *J. Catal.*, 2010, **274**, 200–206.

9 Y. Zhang, Y. Zhou, J. Shi, S. Zhou, X. Sheng, Z. Zhang and S. Xiang, *J. Mol. Catal. A Chem.*, 2014, **381**, 138–147.

10 X. Liu, W. Z. Lang, L. L. Long, C. L. Hu, L. F. Chu and Y. J. Guo, *Chem. Eng. J.*, 2014, **247**, 183–192.

11 O. A. Bariå S, A. Holmen and E. A. Blekkan, *J. Catal.*, 1996, **158**, 1–12.

12 A. A. Castro, *Catal. Letters*, 1993, **22**, 123–133.

13 C. Yu, H. Xu, Q. Ge and W. Li, *J. Mol. Catal. A Chem.*, 2007, **266**, 80–87.

14 Y. ling Shan, Z. J. Sui, Y. A. Zhu, D. Chen and X. G. Zhou, *Chem. Eng. J.*, 2015, **278**, 240–248.

15 R. J. Rennard and J. Freel, *J. Catal.*, 1986, **98**, 235–244.

16 S. B. Kogan, H. Schramm and M. Herskowitz, *Appl. Catal. A Gen.*, 2001, **208**, 185–191.

17 G. Aguilar-Ríos, P. Salas, M. A. Valenzuela, H. Armendáriz, J. A. Wang and J. Salmones, *Catal. Letters*, 1999, **60**, 21–25.

18 D. Pérez-Martínez, S. A. Giraldo and A. Centeno, *Appl. Catal. A Gen.*, 2006, **315**, 35–43.

19 US5336829A, 1994.

20 D. R. Alfonso, *Surf. Sci.*, 2008, **602**, 2758–2768.

21 V. A. Sethuraman and J. W. Weidner, *Electrochim. Acta*, 2010, **55**, 5683–5694.

22 C. R. Apesteguía and J. Barbier, *J. Catal.*, 1982, **78**, 352–359.

23 S. D. Jackson, P. Leeming and J. Grenfell, *J. Catal.*, 1994, **150**, 170–176.

24 C. Gillan, M. Fowles, S. French and S. D. Jackson, *Ind. Eng. Chem. Res.*, 2013, **52**, 13350–13356.

25 R. Mohtadi, W. -k. Lee, S. Cowan, J. W. Van Zee and M. Murthy, *Electrochem. Solid-State Lett.*, 2003, **6**, A272.

26 B. D. Gould, O. A. Baturina and K. E. Swider-Lyons, *J. Power Sources*, 2009, **188**, 89–95.

27 Y. N. Tang, Z. Y. Liu, W. G. Chen, Z. G. Shen, C. G. Li and X. Q. Dai, *Int. J.*

Hydrogen Energy, 2015, **40**, 6942–6949.

28 L. Shi, G. M. Deng, W. C. Li, S. Miao, Q. N. Wang, W. P. Zhang and A. H. Lu, *Angew. Chemie - Int. Ed.*, 2015, **54**, 13994–13998.

29 A. Bazyari, Y. Mortazavi, A. A. Khodadadi, L. T. Thompson, R. Tafreshi, A. Zaker and O. T. Ajenifujah, *Appl. Catal. B Environ.*, 2016, **180**, 312–323.

30 H. Z. Wang, L. L. Sun, Z. J. Sui, Y. A. Zhu, G. H. Ye, D. Chen, X. G. Zhou and W. K. Yuan, *Ind. Eng. Chem. Res.*, 2018, **57**, 8647–8654.

31 Z. P. Han, S. R. Li, F. Jiang, T. Wang, X. Bin Ma and J. L. Gong, *Nanoscale*, 2014, **6**, 10000–10008.

32 Y. Q. Cao, Z. J. Sui, Y. A. Zhu, X. G. Zhou and D. Chen, *ACS Catal.*, 2017, **7**, 7835–7846.

33 M. L. Yang, Y. A. Zhu, X. G. Zhou, Z. J. Sui and D. Chen, *ACS Catal.*, 2012, **2**, 1247–1258.

34 G. Kresse and J. Hafner, *Phys. Rev. B*, 1993, **48**, 13115.

35 G. Kresse and J. Furthmüller, *Phys. Rev. B*, 1996, **54**, 11169–11186.

36 P. E. Blöchl, *B, Phys. Rev.*, 1994, **50**, 17953–17979.

37 J. Barbier, *Stud. Surf. Sci. Catal.*, 1987, **34**, 1–19.

38 S. He, C. Sun, X. Yang, B. Wang, X. Dai and Z. Bai, *Chem. Eng. J.*, 2010, **163**, 389–394.

39 S. Saerens, M. K. Sabbe, V. V. Galvita, E. A. Redekop, M. F. Reyniers and G. B. Marin, *ACS Catal.*, 2017, **7**, 7495–7508.

40 T. Sato, K. Okaya, K. Kunimatsu, H. Yano and H. U. Masahiro Watanabe, *ACS*

Catal., 2012, **2**, 450–455.

41 G. J. Arteaga, J. A. Anderson and C. H. Rochester, *Catal. Letters*, 1999, **58**, 189–194.

42 E. Ivanova, M. Mihaylov, F. Thibault-Starzyk, M. Daturi and K. Hadjiivanov, *J. Mol. Catal. A Chem.*, 2007, **274**, 179–184.

43 F. Jiang, L. Zeng, S. R. Li, G. Liu, S. P. Wang and J. L. Gong, *ACS Catal.*, 2015, **5**, 438–447.

44 G. Bergeret and P. Gallezot, *J. Catal.*, 1984, **87**, 86–92.

45 W. Shi, B. Yi, M. Hou, F. Jing, H. Yu and P. Ming, 2007, **164**, 272–277.

46 H. Wakita, Y. Kani, K. Ukai, T. Tomizawa, T. Takeguchi and W. Ueda, *Appl. Catal. A Gen.*, 2005, **283**, 53–61.

47 P. Biloen, F. M. Dautzenberg and W. M. H. Sachtler, *J. Catal.*, 1977, **50**, 77–86.

48 Z. J. Sui, Y. A. Zhu, P. Li, X. G. Zhou and D. Chen, *Kinetics of catalytic dehydrogenation of propane over Pt-based catalysts*, Elsevier Inc., 1st edn., 2014, vol. 44.

49 M. P. Lobera, C. Téllez, J. Herguido, Y. Schuurman and M. Menéndez, *Chem. Eng. J.*, 2011, **171**, 1317–1323.

50 M. L. Yang, J. Zhu, Y. A. Zhu, Z. J. Sui, Y. Da Yu, X. G. Zhou and D. Chen, *J. Mol. Catal. A Chem.*, 2014, **395**, 329–336.

51 A. Michaelides and P. Hu, *J. Chem. Phys.*, 2001, **115**, 8570–8574.

52 D. C. Chen, X. X. Zhang, J. Tang, J. N. Fang, Y. Li and H. J. Liu, *Appl. Phys.*

A Mater. Sci. Process., 2018, **124**, 0.

53 J. Sivek, H. Sahin, B. Partoens and F. M. Peeters, *Phys. Rev. B - Condens. Matter Mater. Phys.*, 2013, **87**, 1–8.

54 Q. Yue, Z. Shao, S. Chang and J. Li, *Chem. Phys. Lett.*, 2013, 1–7.

55 Y. N. Tang, L. J. Pan, W. G. Chen, Z. G. Shen, C. G. Li and X. Q. Dai, *Compos. Interfaces*, 2016, **23**, 423–432.

56 X. Chu, Z. Lu, Y. Zhang and Z. Yang, *Int. J. Hydrogen Energy*, 2013, **38**, 8974–8979.

57 H. Orita, N. Itoh and Y. Inada, *Surf. Sci.*, 2004, **571**, 161–172.

58 G. Kresse, A. Gil and P. Sautet, *Phys. Rev. B - Condens. Matter Mater. Phys.*, 2003, **68**, 3–6.

59 M. L. Yang, Y. A. Zhu, C. Fan, Z. J. Sui, D. Chen and X. G. Zhou, *J. Mol. Catal. A Chem.*, 2010, **321**, 42–49.

60 B. K. Vu, M. B. Song, I. Y. Ahn, Y. W. Suh, D. J. Suh, W. Il Kim, H. L. Koh, Y. G. Choi and E. W. Shin, *Appl. Catal. A Gen.*, 2011, **400**, 25–33.

61 J. F. Yu, R. Wang, S. Y. Ren, X. Y. Sun, C. L. Chen, Q. jJe Ge, W. Fang, J. Zhang, H. Y. Xu and D. S. Su, *Unique Role CaO Stab. Pt/Al2O3 Catal. Dehydrogenation Cyclohexane*, 2012, **4**, 1376–1381.

62 M. L. Yang, Y. A. Zhu, C. Fan, Z. J. Sui, D. Chen and X. G. Zhou, *Phys. Chem. Chem. Phys.*, 2011, **13**, 3257–3267.

63 Y. L. Shan, Y. A. Zhu, Z. J. Sui, D. Chen and X. G. Zhou, *Catal. Sci. Technol.*, 2015, **5**, 3991–4000.